DOI: 10.1002/chem.200901216

Fullerene Derivatives Functionalized with Diethylamino-Substituted Conjugated Oligomers: Synthesis and Photoinduced Electron Transfer

Aline Gégout,[a, b] Jean-François Nierengarten,*[a] Béatrice Delavaux-Nicot,*[b] Carine Duhayon,[b] Alix Saquet,[b] Andrea Listorti,[c] Abdelhalim Belbakra,[c] Claudio Chiorboli,[d] and Nicola Armaroli*[c]

In memory of Jean-Marie Nierengarten

Abstract: Diethylamino-substituted oligophenylenevinylene (OPV) building blocks have been prepared and used for the synthesis of two [60]fullerene–OPV dyads, **F-D1** and **F-D2**, which exhibit different conjugation length of the OPV fragments. The electrochemical properties of these acceptor–donor dyads have been studied by cyclic voltammetry. The first reduction is always assigned to the fullerene moiety and the first oxidation centered on the diethylaniline groups of the OPV rods, thus making these systems suitable candidates for photoinduced electron transfer. Both the OPV and the fullerene-centered fluorescence bands are quenched in toluene and benzonitrile, which suggests the occurrence of photoinduced electron transfer from the amino-substituted OPVs to the carbon sphere in the dyads in both solvents. By means of bimolecular quenching experiments, transient absorption spectral fingerprints of the radical cationic species are detected in the visible (670 nm) and near-IR (1300–1500 nm) regions, along with the much weaker fullerene anion band at $\lambda_{max} = 1030$ nm. Definitive evidence for photoinduced electron transfer in **F-D1** and **F-D2** comes from transient absorption measurements. A charge-separated state is formed within 100 ps and decays in less than 5 ns.

Keywords: electrochemistry · electron transfer · fullerenes · oligophenylenevinylene · photophysics

[a] Dr. A. Gégout, Prof. Dr. J.-F. Nierengarten
Laboratoire de Chimie des Matériaux Moléculaires
Université de Strasbourg et CNRS (UMR 7509)
Ecole Européenne de Chimie, Polymères et Matériaux (ECPM)
25 rue Becquerel, 67087 Strasbourg Cedex 2 (France)
Fax: (+33) 3-90-242-774
E-mail: nierengarten@chimie.u-strasbg.fr

[b] Dr. A. Gégout, Dr. B. Delavaux-Nicot, Dr. C. Duhayon, Dr. A. Saquet
Laboratoire de Chimie de Coordination du CNRS
205 route de Narbonne, 31077 Toulouse Cedex 4 (France)
Fax: (+33) 5-61-55-30-03
E-mail: beatrice.delavaux-nicot@lcc-toulouse.fr

[c] Dr. A. Listorti, A. Belbakra, Dr. N. Armaroli
Molecular Photoscience Group
Istituto per la Sintesi Organica e la Fotoreattività
Consiglio Nazionale delle Ricerche
via Gobetti 101, 40129 Bologna (Italy)
Fax: (+39) 051-6399844
E-mail: nicola.armaroli@isof.cnr.it

[d] Dr. C. Chiorboli
Istituto per la Sintesi Organica e la Fotoreattività
Consiglio Nazionale delle Ricerche, Sezione di Ferrara
via Borsari 46, 44100 Ferrara (Italy)

Introduction

Owing to their potential for photovoltaic applications,[1] hybrid compounds combining fullerene with π-conjugated oligomers have generated intense research activities in the past few years.[2] In addition, C_{60}–(π-conjugated oligomer) hybrid systems also offer interesting perspectives for optical limiting or photodynamic therapy applications.[3] The peculiar electronic properties of C_{60}–(π-conjugated oligomer) dyads led to the development of dendritic systems with interesting light-harvesting properties[4] or used for evidencing original dendritic effects.[5] As part of this research, we have designed numerous C_{60}–oligophenylenevinylene (C_{60}–OPV) dyads and studied systematically their electronic properties.[6] As far as their photophysical properties are concerned, a characteristic feature in all these systems is an ultrafast energy transfer from the lowest singlet excited state of the OPV-conjugated system to populate the fullerene singlet.[6] This first event can be followed by an electron transfer, depending on the donating ability of the OPV oligomer, on structural factors, and on the solvent polarity.[6,7] Actual-

ly, for C_{60}–OPV conjugates combining the fullerene-accepting unit with relatively short OPV oligomers, the charge-separated state is higher in energy than the first fullerene singlet excited state, no matter what the conditions.[6] In this case, the light energy absorbed by the conjugated system is promptly conveyed to the fullerene lowest singlet excited state by means of energy transfer and no longer yields charge separation. By increasing the length of the OPV-conjugated backbone and thus its donating ability, dramatic effects of the solvent polarity have been observed upon photoexcitation of the OPV moiety.[6,7] In apolar solvents, the charge-separated state is still higher in energy than the first fullerene singlet excited state and no charge separation could be evidenced. In contrast, the situation is completely different in more polar solvents. Effectively, since the energy of the charge-separated state drops below that of the first fullerene singlet excited state, electron transfer is observed upon the initial singlet energy-transfer event. Similar findings have been reported by Martin, Guldi, and co-workers[8] for a series of oligonaphthylenevinylene–fullerene dyads. In this paper, we now report the synthesis and the electronic properties of two new C_{60}–OPV dyads. Owing to the presence of diethylamino substituents on the OPV fragments, their donating ability has been improved. In this way, the energy level of the charge-separated state is significantly lower in energy. As a result, the thermodynamic driving force is more favorable and electron transfer occurs whatever the solvent.

Results and Discussion

Synthesis: The synthesis of the C_{60}–OPV conjugates is based on the esterification reaction of a fullerene carboxylic acid building block with OPV oligomers bearing one hydroxy group. To this end, we have first prepared alcohols **5** and **10** (Schemes 1 and 2). The synthetic approach to preparing the conjugated backbone of both building blocks relies upon reaction of phosphonate **3** and a bis-aldehyde derivative. Indeed, the Wadsworth–Emmons reaction has proven to be a powerful tool for the synthesis of OPV derivatives as the *trans* olefines are selectively produced from benzylic phosphonates.[9]

Phosphonate **3** was obtained in two steps from commercially available aldehyde **1** (Scheme 1). Reduction of **1** with lithium aluminum hydride ($LiAlH_4$) in THF gave alcohol **2** in 99% yield. The preparation of phosphonate **3** was then achieved from benzylic alcohol **2** under the reaction conditions developed by Marder and co-workers.[10] Actually, benzylic phosphonate is usually prepared by halogenation of the benzylic alcohol followed by treatment with $P(OEt)_3$ under Arbuzov conditions. This route, however, is not appropriate when starting from electron-rich benzylic alcohol derivatives such as **2** owing to the instability of the corresponding benzylic halide. The choice of the appropriate conditions for the preparation of phosphonate **3** was indeed the key to this synthesis. Under Marder conditions using I_2 and

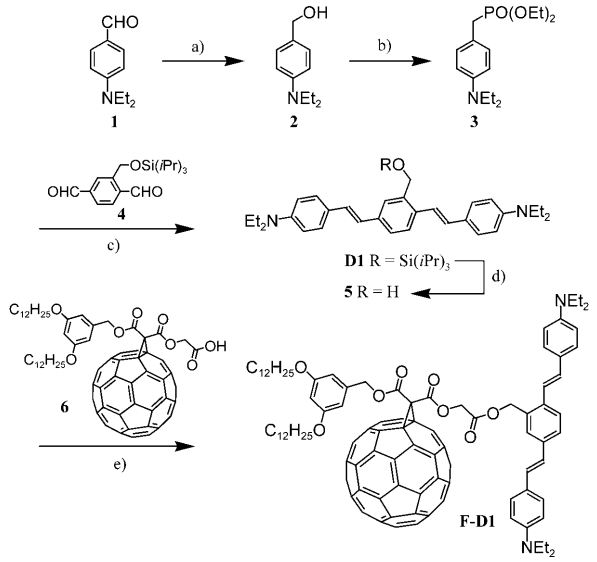

Scheme 1. Reagents and conditions: a) $LiAlH_4$, THF, 0°C (99%); b) I_2, $P(OEt)_3$, 0°C to RT (45%); c) *t*BuOK, THF, 0°C to RT (42%); d) TBAF, THF, 0°C (80%); e) DCC, DMAP, CH_2Cl_2, 0°C to RT (70%).

$P(OEt)_3$, phosphonate **3** was directly obtained from alcohol **2** in 45% yield. Reaction of **3** with dialdehyde **4**[11] in the presence of *t*BuOK in THF afforded the OPV model compound **D1** in 42% yield. All the spectroscopic studies and elemental analysis results were consistent with the structure of **D1**. In particular, coupling constants of approximately 16 Hz for the AB systems corresponding to the signals of the vinylic protons in the ^1H NMR spectrum were in good agreement with the *E* stereochemistry of all the double bonds in **D1**. This was further confirmed by the X-ray crystal-structure analysis of compound **D1** (Figure 1). Interestingly, the conjugated backbone of **D1** adopts a twisted conformation in the solid state, with an angle of approximately 70° being observed between the planes of the two terminal aromatic rings (A and C). The peculiar twist of the OPV core can be easily explained by close inspection of the packing. Observation of the crystal lattice down the crystallographic axis *a* reveals a layered structure in which the molecules aligned with axis *b* are arranged alternatively up and down along axis *c*. As shown in Figure 1, the twisting of the conjugated system results from the presence of the bulky triisopropylsilyl (TIPS) groups of the neighboring molecules. Furthermore, this twist allows the establishment of an attractive intermolecular CH–π interaction between one C–H of phenyl unit C and the aromatic ring A of its neighboring molecule (not shown).

Treatment of **D1** with tetra-*n*-butylammonium fluoride (TBAF) in THF at 0°C afforded alcohol **5**. Finally, *N*,*N*′-dicyclohexylcarbodiimide (DCC)-mediated esterification of **5** with carboxylic acid **6**[12] yielded dyad **F-D1**. The structure and purity of compound **F-D1** were confirmed by ^1H and ^{13}C NMR spectroscopy, mass spectrometry, and elemental analysis.

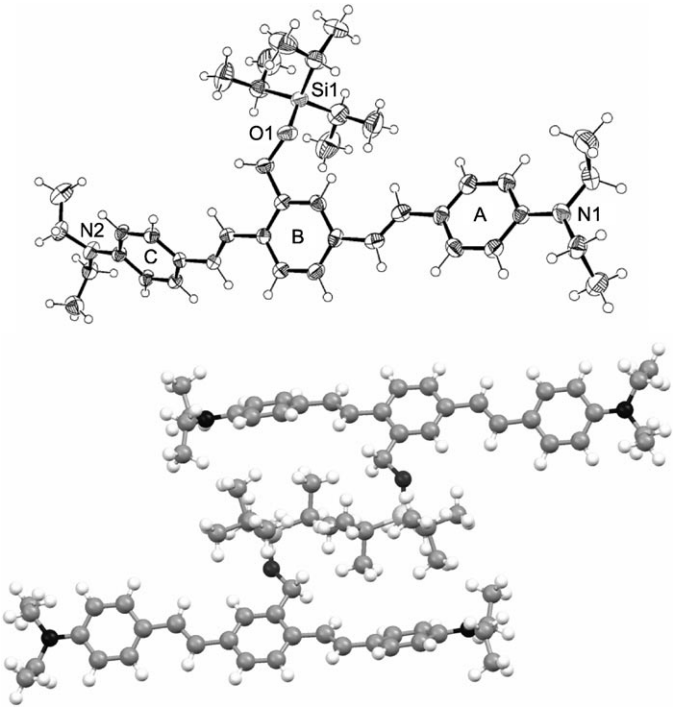

Figure 1. Top: ORTEP plot of the structure of **D1** (thermal ellipsoids are drawn at the 50% probability level). Bottom: stacking within the **D1** lattice (view down the crystallographic axis *a*).

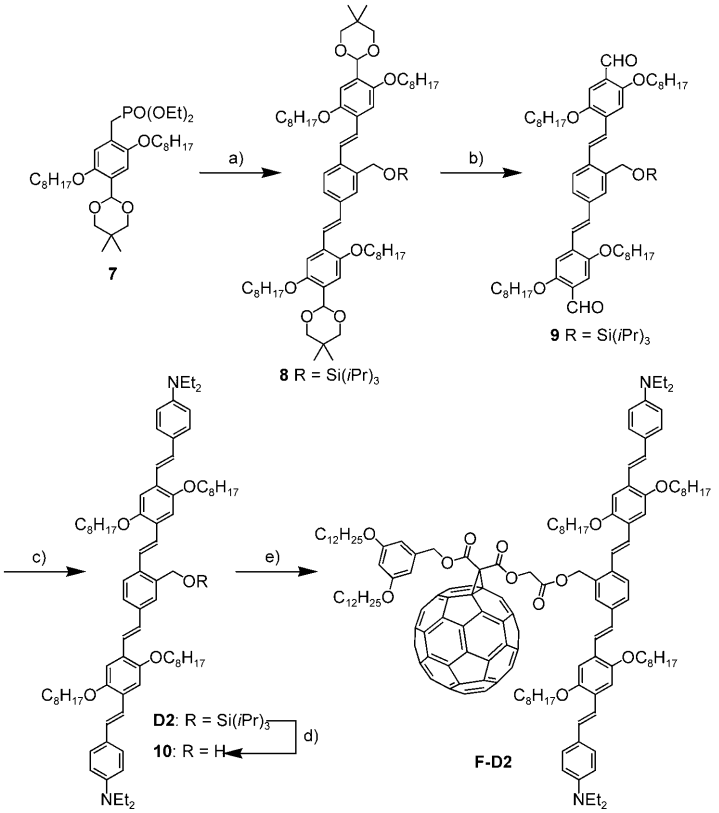

Scheme 2. Reagents and conditions: a) **4**, *t*BuOK, THF, 0°C to RT (73%); b) CF_3CO_2H, CH_2Cl_2, H_2O, RT (76%); c) **3**, *t*BuOK, THF, 0°C to RT (33%); d) TBAF, THF, 0°C (70%); e) **6**, DCC, DMAP, CH_2Cl_2, 0°C to RT (60%).

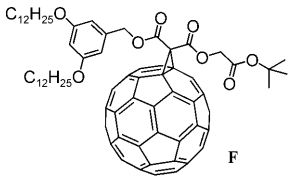

The preparation of the second dyad with an OPV pentameric subunit is depicted in Scheme 2. Reaction of dialdehyde **4** with phosphonate **7** gave OPV trimer **8** in 73% yield. Subsequent treatment with CF_3CO_2H in CH_2Cl_2/H_2O afforded dialdehyde **9** in 76% yield. The TIPS-protected OPV pentamer **D2** was then prepared under Wadsworth–Emmons conditions from dialdehyde **9** and phosphonate **3**. The moderate yield for this step (33%) is mainly associated with difficulties encountered during the purification of **D2**. Alcohol **10** was obtained in 70% yield by treatment with TBAF in THF at 0°C. Reaction of **10** with carboxylic acid **6** under esterification conditions using DCC and 4-dimethylaminopyridine (DMAP) afforded compound **F-D2** in 60% yield. Owing to the presence of the alkyloxy groups, compound **F-D2** is highly soluble in common organic solvents (CH_2Cl_2, $CHCl_3$, benzene, toluene, THF) and was thus easily characterized by FTIR, ^{1}H NMR, and ^{13}C NMR spectroscopies. The structure of **F-D2** was also confirmed by its MALDI-TOF mass spectrum showing the expected molecular ion peak at *m*/*z* 2493.0 ($[M]^+$; *m*/*z* calcd for $C_{175}H_{170}N_2O_{12}$: 2493.28).

Electrochemistry: The electrochemical properties of hybrid compounds **F-D1** and **F-D2** were investigated by cyclic voltammetry (CV). For the sake of comparison, electrochemical measurements were also carried out with model compounds **D1**, **D2**, and **F**. All the experiments were performed at room temperature on solutions of the samples in CH_2Cl_2 containing tetra-*n*-butylammonium tetrafluoroborate (0.1 M) as supporting electrolyte, with a Pt wire as the working electrode and a saturated calomel electrode (SCE) as a reference. Potential data for all of the compounds are collected in Table 1. As a typical example, the cyclic voltammogram obtained from **F-D2** is shown in Figure 2.

Table 1. Electrochemical data of **F**, **D1**, **D2**, **F-D1**, and **F-D2** determined by CV on a Pt working electrode in CH_2Cl_2/0.1 M nBu_4NBF_4 at room temperature.

	Oxidation	Reduction			
	E_1[a]	E_1[a]	E_2[b]	E_3[b]	E_4[b]
F	–	−0.51	−0.89	−1.11	−1.36
D1	+0.59[c]	–	–	–	–
F-D1	+0.62[c]	−0.53	−0.90	−1.12	−1.37
D2	+0.59[c]	–	–	–	–
F-D2	+0.61[c]	−0.51	−0.88	−1.12	−1.37

[a] Values for $(E_{pa}+E_{pc})/2$, in which E_{pa} and E_{pc} are the oxidation and reduction peak values, respectively, in V versus SCE at a scan rate of 0.1 Vs^{-1}. [b] Peak potential value at a scan rate of 0.1 Vs^{-1}, irreversible process. [c] Bielectronic process.

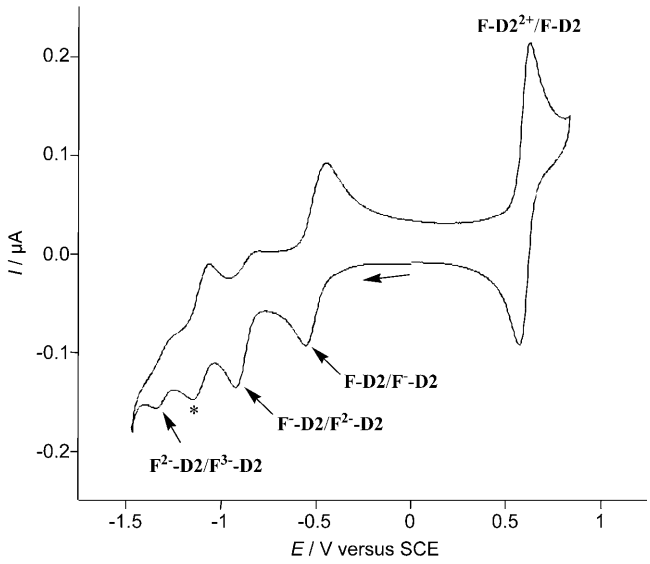

Figure 2. Cyclic voltammogram of compound **F-D2** on a Pt electrode at $v=0.1\ Vs^{-1}$ in CH_2Cl_2/0.1 M nBu_4NBF_4 (* indicates the reduction of an electrogenerated species, see text).

In the cathodic region, compound **F** shows the classical behavior observed for methanofullerene derivatives.[13] Whereas the first reduction observed at −0.59 V versus SCE is always reversible, the second is irreversible at low scan rates but becomes reversible upon increasing the scan rate. The third wave gradually disappears when the second one becomes reversible, so that it likely implies reduction of the product formed after the second reduction.[13,14] Indeed, a bond breaking in the cyclopropane ring upon the second reduction may explain this peculiar behavior, as already reported for several methanofullerene derivatives.[15] Finally, the reduction observed at −1.36 V versus SCE corresponds to the redox couple C_{60}^{3-}/C_{60}^{2-}. In the anodic region, model compound **F** presents an irreversible peak at +1.66 V versus SCE, which can be likely attributed to the oxidation of the dialkyloxyphenyl unit.[16] In the anodic region, both oligomers **D1** and **D2** exhibit a reversible two-electron transfer process at +0.59 V versus SCE centered on the diethylaniline subunits.[17] Indeed, in both cases, the two terminal diethylaniline subunits are oxidized at the same potential. Irreversible reduction processes were also observed at −1.82 and −2.18 V versus SCE for **D2** and **D1**, respectively. The cyclic voltammograms recorded for hybrid compounds **F-D1** and **F-D2** shows the characteristic electrochemical features of both constitutive units (i.e., methanofullerene and OPV). The comparison of the $E_{1/2}$ potentials of **F-D1** and **F-D2** with the corresponding model compounds clearly shows that, for both hybrid compounds, the four first reduction waves correspond to fullerene-centered processes, whereas the oxidation process is centered on the conjugated OPV backbone. Comparison of the redox potentials of **F-D1** and **F-D2** with those of the corresponding model compounds **D1** and **D2** reveals that the oxidation potential of both moieties are slightly shifted to more positive values. This shift could be a consequence of small electronic interactions between the OPV core and the C_{60} units, resulting in a more difficult oxidation for the OPV subunit. However, for both **F-D1** and **F-D2**, the different subunits are separated by rather long spacers and the photophysical studies revealed no particular ground-state electronic interactions (vide infra). Therefore, it appears more reasonable to ascribe the observed potential shift to solvation effects resulting from the presence of the surrounding apolar fullerene groups as already reported to explain slight potential changes of related C_{60}–OPV conjugates.[6,11]

Ground-state absorption and luminescence properties: The electronic absorption spectra of dyads **F-D1** and **F-D2** in toluene are reported in Figure 3a. Peaks at $\lambda<350$ nm are attributable to the fullerene moiety, whereas the lowest energy absorption band is due to the OPV fragment, red-shifted in the case of the pentamer (**F-D2**), which is characterized by a more extensive conjugation.[18] The absorption spectra of both dyads exhibit minor differences when compared with the sum of the spectra of the related reference compounds, indicating negligible ground-state electronic interactions.

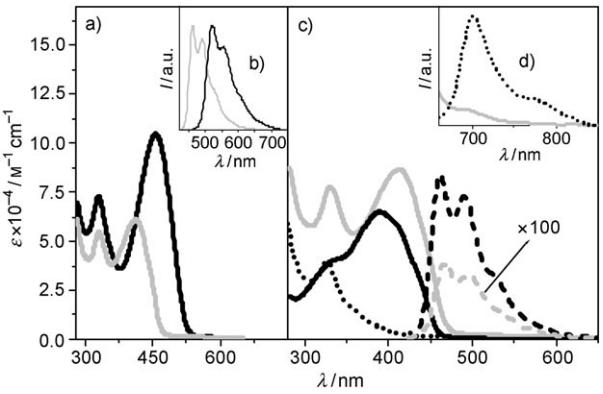

Figure 3. a) Absorption spectra of **F-D1** (gray) and **F-D2** (black) in toluene at 298 K. b) Normalized fluorescence spectra of **D1** (gray) and **D2** (black) in toluene at $\lambda_{exc}=400$ nm. c) Absorption spectra of **F-D1** (gray) and its constituents **D1** (black) and **F** (dotted black); the dashed lines represent the OPV-centered fluorescence bands of **F-D1** (gray) and **D1** (black) in toluene at $\lambda_{exc}=400$ nm. d) Fullerene-centered fluorescence spectra: **F** (dotted black) and **F-D1** (gray) in toluene at $\lambda_{exc}=550$ nm.

As typically observed for OPV-type molecules, **D1** and **D2** exhibit intense and short-lived emission (Table 2, Figure 3b), attributable to deactivation of the lowest singlet

Table 2. Fluorescence data of solutions of the compounds in toluene.

	298 K			77 K
	λ_{max} [nm]	τ [ns]	ϕ	λ_{max} [nm]
D1	461	0.9	0.43	470
D2	521	1.0	0.49	534
F-D1	471	<0.5	0.003	473
F-D2	527	<0.5	0.03	545

electronic level.[7,19] This fluorescence signal is substantially quenched in all dyads, suggesting the occurrence of OPV–C_{60} excited-state interactions (Table 2, Figure 3c). As extensively discussed in the past for similar OPV–C_{60} structures, the quenching mechanism is ultrafast ^{1}OPV$\rightarrow^1C_{60}$ singlet energy transfer.[5,6,20] Importantly, sensitization of the carbon sphere through the OPV moiety ($\lambda_{exc}=450$ nm) or direct excitation of the fullerene singlet level ($\lambda_{exc}=550$ nm) does not result in any fullerene fluorescence even in apolar toluene (see Figure 3d as an example). Moreover, no singlet oxygen-sensitized emission is detected in the near-IR at 1270 nm, also ruling out the population of the fullerene triplet level for both **F-D1** and **F-D2**. These results can be rationalized by assuming that the electronic excited states centered on the two moieties are quenched due to the presence of a low-lying charge-separated state indicated as $\mathbf{F}^-$–$\mathbf{D}^+$, with the positive charge being located on the terminal amine residue of the OPV moiety. This is also in line with findings reported by Martin, Guldi, and co-workers on a series of fullerene derivatives substituted with conjugated dendritic wedges functionalized with peripheral dibutylaniline subunits.[4f]

Transient absorption spectroscopy: To get evidence for the occurrence of photoinduced electron transfer, transient absorption investigations were first accomplished by means of bimolecular quenching experiments, with the aim of revealing the spectral features of the involved cationic and anionic species. Experiments were carried out both in toluene and in more polar benzonitrile and the results obtained are virtually identical. Figure 4a depicts the transient absorption spectra in the nano- and microsecond timescale obtained with a solution of **F** (0.1 mM) in the presence of **D2** (0.1 mM)

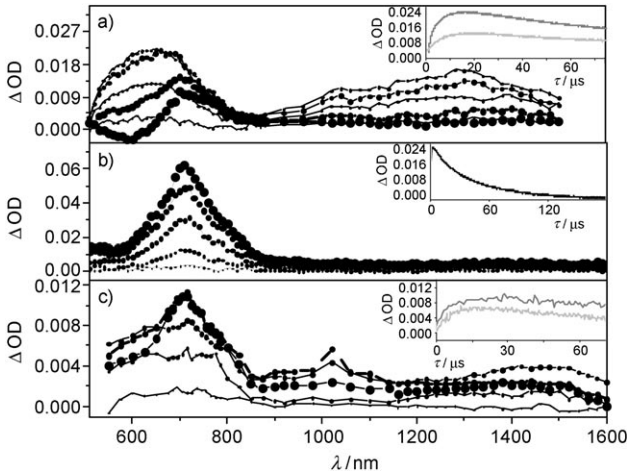

Figure 4. Transient absorption spectra of oxygen-free benzonitrile containing a) **F** and **D2** and c) **F** and **D1**, at 1×10^{-4} M. Depicted spectral traces are at 1, 2, 11, 70, 170, and 350 μs (from bigger to smaller circles) after the laser pulse. Insets: absorbance decay at 710 (black), 600 (gray), and 1020 nm (light gray). $\lambda_{exc}=532$ nm. Energy: 0.5 mJ per pulse. b) Reference transient absorption spectra of oxygen-free benzonitrile containing **F**. Depicted spectral traces are taken between 1 and 80 μs (from bigger to smaller circles). Inset: absorbance decay at 700 nm. $\lambda_{exc}=$ 532 nm; energy: 0.5 mJ per pulse.

in oxygen-free benzonitrile (BN). The broad absorption band with a peak of 700 nm and appearing immediately after the ns-laser pulse is attributed to the fullerene triplet (^{3}**F***);[21] for comparison, see the typical long-lived triplet absorption features of **F** alone in benzonitrile (Figure 4b). The early triplet spectral trace of **F** (700 ns) then disappears and a new spectral profile appears with two broad bands in the visible and near-IR regions at $\lambda_{max}=640$ and 1300 nm. Such bands are assigned to the radical cation of **D2**[22] and their rise occurs within about 15 μs after excitation (Figure 4a, inset). By adding oxygen to the solution, in which an intermolecular energy transfer from $^3C_{60}$* to oxygen takes place,[23,24] the electron-transfer event is suppressed and the novel spectral traces are no longer detected, confirming the occurrence of electron transfer from the fullerene triplet level. Despite several efforts, a detailed Stern–Volmer kinetic analysis of the bimolecular quenching process with determination of the electron-transfer yield (Φ_{et}) and rate (k_{et}),[22,24,25] was not possible due to the substantial overlapping of the fullerene triplet spectral features with the intense radical cation bands, which prevents a reliable evaluation of the pseudo-first-order decay-rate constant of ^{3}F*. The strong intensity of the radical cation band of **D2** also masks the weak radical anion feature of methanofullerene above 1000 nm[26] (Figure 4a). However, in an attempt to observe this band, which can serve as final evidence for electron transfer, bimolecular quenching experiments were also carried out with **D1**. In this case, the near-IR cationic peak in the near-IR region is shifted to 1500 nm and the fingerprint of the fullerene radical anion was unambiguously observed at 1020 nm (Figure 4c).

Transient absorption spectra were then recorded for both **F-D1** and **F-D2** in deaerated benzonitrile and toluene on the ns–μs timescale. However, no transient absorption spectral traces of any sort (including fullerene triplet) can be detected in either solvent with nanosecond resolution. This suggests that the forward- and back-electron transfer processes occur on a shorter timescale. The fast charge-recombination process is ascribable to the short distance (both through bond and through space) between the donor and acceptor moieties in both **F-D1** and **F-D2** dyads.

To get a clearer picture of the photoinduced processes occurring in both **F-D1** and **F-D2**, transient absorption investigations were carried out on samples in toluene using a femtosecond laser apparatus. The two dyads excited at 550 nm show, immediately after the excitation pulse, an intense and broad absorption feature with a maximum at 740 nm and a lifetime of 36 and 60 ps for **F-D1** and **F-D2**, respectively (Figure 5). A broad band is then detected at longer times with a maximum around 700 nm, which does not decay in the time window of the ultrafast spectrometer (1 ns). This latter band looks quite similar to that observed in bimolecular experiments on the nanosecond timescale (Figure 4a and c) and is assigned to the cation of the OPV donor moiety. In summary, a forward photoinduced electron-transfer process is observed within 60 ps and the related charge-separated state exists more than 1 ns. Moreover, the aforementioned

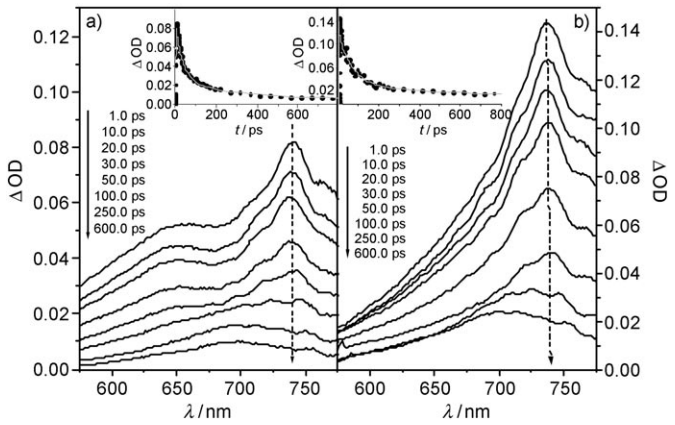

Figure 5. Ultrafast transient absorption spectra of a) **F-D1** and b) **F-D2** in toluene (1×10^{-4} M); $\lambda_{exc}=550$ nm. Energy: 20 μJ per pulse. Inset: Decay kinetics recorded at 740 nm.

lack of signals attributable to radical-ion species in nanosecond transient absorption experiments, throughout the visible/near-IR region, suggests that the back-electron transfer process occurs at time shorter than 5 ns (nanosecond apparatus time resolution). Accordingly, the charge-separated state is estimated to exist between 1 and 5 ns in toluene solution.

To find out the excited levels involved in the formation of the charge-separated state, we also investigated the transient absorption behavior of **F**, **D1**, and **F-D1** upon ultrafast excitation (Figure 6). This allowed us to unambiguously assign

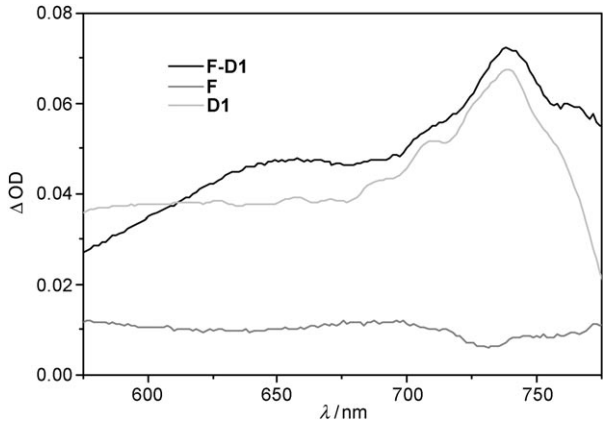

Figure 6. Transient absorption spectra of **F** (dark gray), **D1** (light gray), and **F-D1** (black) recorded immediately after the laser pulse ($\lambda_{exc}=$ 550 nm). Energy: 20 μJ per pulse.

the absorption band shown by the dyads (Figure 5) at 740 nm to the singlet excited state of the OPV moieties. For **D1** and **D2**, transient absorption traces decrease on a much longer time scale (ns); this is in agreement with the observed fluorescence decays.

The precise pathway of excited-state deactivation following light excitation of **F-D1** and **F-D2** cannot be completely disclosed. Indeed, after the fast formation of the OPV singlet state no intermediates are clearly identified. This could be due to a strong difference in the absorption coefficient values and a partial superimposition of the radical-ion absorption features compared with the singlet OPV ones. Accordingly, in principle, population of either singlet and triplet fullerene excited states cannot be excluded. Indeed, photoinduced electron transfer from the fullerene triplet level may lead to the formation of the charge-separated state as demonstrated with bimolecular quenching experiments. However, the rate of formation of the OPV cation in these dyads (36 and 60 ps) indicates a fast electron-transfer process, which rules out the involvement of the fullerene triplet level that is formed on the nanosecond timescale.

Conclusion

We have developed novel diethylamino-substituted OPV derivatives bearing an alcohol group, which allows their further functionalization with a fullerene subunit. The electrochemical properties of the resulting C_{60}–OPV dyads have been investigated. Whereas the first reduction of both C_{60}–OPV conjugates is centered on the C_{60} unit, the first oxidation is assigned to the terminal diethylaniline residues of the OPV rods. Importantly, both OPV derivatives **D1** and **D2** possess excellent donating abilities and appear to be an ideal electron donor for the fullerene acceptor in photoinduced electron transfer. This process has been first unambiguously evidenced by means of bimolecular quenching experiments monitored by transient absorption spectroscopy. Intermolecular photoinduced electron transfer originates from triplet quenching of the reference fullerene molecule (**F**) by **D1** and **D2**. These experiments allow also for the determination of the spectral fingerprints of radical-ion transient species in the visible/near-IR region, which are formed within 15 μs after the laser pulse. An intramolecular photoinduced electron-transfer process has also been evidenced in both dyads by the lack of the typical OPV- and fullerene-centered fluorescence. Photoinduced electron transfer occurs in 36 and 60 ps for **F-D1** and **F-D2**, respectively, and the charge-separated state is evaluated to exist between 1 and 5 ns. In conclusion, the functionalization of the conjugated oligomers with dialkylamino groups is an efficient strategy to promote electron transfer in C_{60}–OPV conjugates. This is an important design principle for the engineering of new molecular photovoltaic materials. The short lifetime of the intramolecular charge-separated state in solution is actually not an obstacle for their photovoltaic applications. Indeed, long-lived charge-separated states are usually evidenced in thin films (millisecond time domain) in strong contrast with the short lifetimes determined in solutions.[7a] This is attributed to the migration of opposite charges to different molecules in the solid state.

Experimental Section

General: Reagents and solvents were purchased as reagent grade and used without further purification. Compounds **4**,[11] **6**,[12] **7**,[27] and **F**[12] were prepared according to the literature. THF was distilled over sodium benzophenone ketyl. All reactions were performed in standard glassware under an inert argon atmosphere. Evaporation and concentration were done at water aspirator pressure and drying in vacuo at 10^{-2} torr. Column chromatography: silica gel 60 (230–400 mesh, 0.040–0.063 mm) was purchased from E. Merck and treated with Et_3N (1% in CH_2Cl_2) for the purification of compounds bearing NEt_2 groups. Thin-layer chromatography (TLC) was performed on glass sheets coated with silica gel 60 F_{254} purchased from E. Merck, visualization by UV light. IR spectra (cm^{-1}) were measured using an ATI Mattson Genesis Series FTIR instrument. NMR spectra were recorded on a Bruker AC 300 with solvent peaks as reference. MALDI-TOF MS were obtained using a Bruker BIFLEX™ mass spectrometer. Elemental analyses were performed by the analytical service at the Institut Charles Sadron, Strasbourg.

Compound 2: A 1 M solution of $LiAlH_4$ in THF (7 mL) was added to a stirred solution of **1** (1.00 g, 5.64 mmol) in dry THF (120 mL) at 0 °C. After 4 h, MeOH was added, then water. The resulting mixture was filtered over Celite and evaporated. Column chromatography (silica gel, CH_2Cl_2/hexane 1:1) yielded **2** (1.01 g, 99%) as a pale bluish oil. $C_{11}H_{17}NO$ (M_r = 179.26); ^{1}H NMR ($CDCl_3$, 300 MHz): δ = 7.24 (d, J = 7 Hz, 2H), 6.62 (d, J = 7 Hz, 2H), 4.55 (s, 2H), 3.35 (q, J = 7 Hz, 4H), 1.17 ppm (t, J = 7 Hz, 6H).

Compound 3: I_2 (1.62 g, 6.39 mmol) was added to a solution of **2** (1.15 g, 6.39 mmol) in $P(OEt)_3$ (11 mL) at 0 °C. After 10 min, the mixture was allowed to slowly warm to room temperature (within 1 h), then stirred for 2 h, and evaporated. The residue was taken up with Et_2O, washed with a saturated aqueous NH_4Cl solution, dried ($MgSO_4$), filtered, and evaporated. Column chromatography (silica gel, CH_2Cl_2/AcOEt 4:1) yielded **3** (861 mg, 45%) as a pale bluish oil. $C_{15}H_{26}NO_3P$ (M_r = 299.35); ^{1}H NMR ($CDCl_3$, 300 MHz): δ = 7.12 (m, 2H), 6.62 (d, J = 7 Hz, 2H), 4.00 (m, 4H), 3.32 (m, 4H), 3.04 (d, J = 21 Hz, 2H), 1.25 (t, J = 7 Hz, 6H), 1.13 ppm (t, J = 7 Hz, 6H).

Compound D1: *t*BuOK (83 mg, 0.74 mmol) was added to a stirred solution of **3** (210 mg, 0.69 mmol) and **4** (100 mg, 0.31 mmol) in THF (15 mL) at 0 °C. After 1 h, the mixture was allowed to slowly warm to room temperature (within 1 h), then stirred for 2 h, filtered, and evaporated. Column chromatography (silica gel, hexane/CH_2Cl_2 4:1) followed by recrystallization in EtOH/$CHCl_3$ yielded **D1** (81 mg, 42%) as yellow crystals. ^{1}H NMR ($CDCl_3$, 300 MHz): δ = 7.65 (s, 1H), 7.56 (d, J = 8 Hz, 1H), 7.39 (d, J = 8 Hz, 4H), 7.35 (d, J = 16 Hz, 1H), 7.06 (d, J = 16 Hz, 1H), 7.05 (d, J = 16 Hz, 1H), 6.97 (s, 1H), 6.89 (d, J = 16 Hz, 1H), 6.67 (d, J = 8 Hz, 4H), 4.96 (s, 2H), 3.39 (m, 8H), 1.19 (t, J = 7 Hz, 12H), 1.13 ppm (m, 21H); ^{13}C NMR ($CDCl_3$, 75 MHz): δ = 128.15, 128.1, 127.9, 127.8, 127.7, 125.0, 124.6, 124.3, 120.2, 120.1, 111.8, 111.7, 63.5, 44.4, 18.2, 12.6, 12.1 ppm; elemental analysis calcd (%) for $C_{40}H_{58}N_2OSi$ (611.00): C 78.63, H 9.57, N 4.58; found: C 78.66, H 10.11, N 4.60.

Compound 5: A 1 M solution of TBAF in THF (0.4 mL) was added to a stirred solution of **D1** (170 mg, 0.27 mmol) in dry THF (5 mL) at 0 °C under argon. After 2 h, H_2O (10 mL) was added. The THF was evaporated and CH_2Cl_2 was added. The organic layer was washed with water, dried ($MgSO_4$), and evaporated. Column chromatography (silica gel, CH_2Cl_2/hexane 2:1) yielded **5** (98 mg, 80%) as an orange glassy product. $C_{31}H_{38}N_2O$ (M_r = 454.66); ^{1}H NMR ($CDCl_3$, 300 MHz): δ = 7.63 (s, 1H), 7.60 (s, 1H), 7.39 (d, J = 7 Hz, 4H), 7.36 (d, J = 16 Hz, 1H), 7.19 (d, J = 16 Hz, 1H), 7.06 (d, J = 16 Hz, 1H), 6.97 (s, 1H), 6.88 (d, J = 16 Hz, 1H), 6.67 (d, J = 8 Hz, 4H), 4.84 (d, J = 6 Hz, 2H), 3.39 (m, 8H), 1.19 ppm (t, J = 7 Hz, 12H); ^{13}C NMR ($CDCl_3$, 75 MHz): δ = 130.6, 128.5, 128.1, 127.8, 126.1, 125.75, 125.7, 125.6, 125.6, 124.9, 123.3, 119.9, 111.7, 63.9, 44.4, 17.7, 12.6, 12.3 ppm.

Compound F-D1: DCC (162 mg, 0.79 mmol) and DMAP (8 mg, 0.07 mmol) were added to a solution of **5** (150 mg, 0.33 mmol) and **6** (486 mg, 0.36 mmol) in CH_2Cl_2 (40 mL) at 0 °C. After 1 h, the mixture was allowed to slowly warm to room temperature. After 2 h, the mixture was filtered and evaporated. Column chromatography (silica gel, CH_2Cl_2/hexane 1:1) followed by gel permeation chromatography (Biorad, Biobeads SX1, CH_2Cl_2) gave **F-D1** (409 mg, 70%) as a dark brown glassy product. ^{1}H NMR ($CDCl_3$, 300 MHz): δ = 7.60 (d, J = 8 Hz, 1H), 7.39 (m, 6H), 7.09 (d, J = 16 Hz, 1H), 7.05 (d, J = 16 Hz, 1H), 6.97 (d, J = 16 Hz, 1H), 6.88 (s, 1H), 6.64 (br d, J = 8 Hz, 4H), 6.56 (d, J = 2 Hz, 2H), 6.37 (t, J = 2 Hz, 1H), 5.43 (s, 2H), 5.34 (s, 2H), 5.03 (s, 2H), 3.85 (t, J = 7 Hz, 4H), 3.37 (m, 8H), 1.71 (m, 4H), 1.25 (m, 36H), 1.16 (2t, J = 7 Hz, 12H), 0.88 ppm (t, J = 7 Hz, 6H); ^{13}C NMR ($CDCl_3$, 75 MHz): δ = 166.5, 163.0, 160.4, 147.6, 147.4, 145.2, 145.15, 145.1, 145.0, 144.9, 144.7, 144.6, 144.5, 144.4, 143.8, 143.8, 143.0, 142.95, 142.9, 142.8, 142.2, 142.1, 141.85, 141.8, 140.9, 140.7, 139.8, 138.4, 136.9, 136.7, 136.1, 131.3, 131.27, 128.9, 128.2, 127.9, 126.4, 125.7, 122.9, 119.2, 111.7, 107.3, 101.7, 71.2, 69.0, 68.1, 66.1, 62.7, 44.4, 31.9, 29.7, 29.65, 29.5, 29.4, 29.3, 26.1, 22.7, 14.1, 12.7 ppm; IR (neat): $\tilde{\nu}$ = 1747 cm^{-1} (C=O); MALDI-TOF MS: m/z: calcd for $C_{127}H_{95}N_2O_8$: 1775.71; found: 1775.4 $[M+H]^+$; elemental analysis calcd (%) for $C_{127}H_{94}N_2O_8$ (1776.15): C 85.88, H 5.33, N 1.58; found: C 85.95, H 5.27, N 1.50.

Compound 8: As described for **D1**, with **4** (400 mg, 1.25 mmol), **7** (1.60 g, 2.75 mmol), and *t*BuOK (340 mg, 3.00 mmol). Column chromatography on silica gel (CH_2Cl_2/hexane 3:2) yielded **8** (1.10 g, 73%) as an orange glassy product. $C_{76}H_{124}O_9Si$ (M_r = 1209.90); ^{1}H NMR ($CDCl_3$, 300 MHz): δ = 7.68 (d, J = 8 Hz, 1H), 7.67 (s, 1H), 7.57 (d, J = 16 Hz, 1H), 7.48 (m, 2H), 7.41 (d, J = 16 Hz, 1H), 7.34 (s, 1H), 7.33 (s, 1H), 7.27 (d, J = 16.5 Hz, 1H), 7.18 (s, 1H), 7.17 (s, 1H), 5.74 (s, 2H), 4.94 (s, 2H), 4.03 (t, J = 7 Hz, 4H), 3.98 (t, J = 7 Hz, 4H), 3.72 (AB, J = 11 Hz, 8H), 1.83 (m, 8H), 1.34 (m, 40H), 1.10 (m, 21H), 0.88 (m, 18H), 0.80 ppm (s, 6H).

Compound 9: A mixture of **8** (1.00 g, 0.83 mmol), CH_2Cl_2 (5 mL), CF_3CO_2H (4 mL), and H_2O (5 mL) was vigorously stirred at room temperature for 2 h. The organic layer was then washed with H_2O, dried ($MgSO_4$), and evaporated. A rapid filtration on silica gel (CH_2Cl_2/hexane 1:1) yielded **9** (650 mg, 76%) as an orange-red glassy product. ^{1}H NMR ($CDCl_3$, 300 MHz): δ = 10.48 (s, 2H), 7.68 (d, J = 8 Hz, 1H), 7.67 (s, 1H), 7.57 (d, J = 16 Hz, 1H), 7.48 (m, 2H), 7.41 (d, J = 16 Hz, 1H), 7.34 (s, 1H), 7.33 (s, 1H), 7.27 (d, J = 16,5 Hz, 1H), 7.18 (s, 1H), 7.17 (s, 1H), 4.97 (s, 2H), 4.08 (m, 8H), 1.85 (m, 8H), 1.30 (m, 40H), 1.10 (m, 21H), 0.88 ppm (m, 12H); ^{13}C NMR ($CDCl_3$, 75 MHz): δ = 189.2, 156.2, 150.85, 150.8, 139.2, 136.9, 135.4, 134.4, 134.3, 132.1, 128.7, 126.2, 126.0, 125.9, 124.8, 124.4, 124.3, 123.1, 110.8, 110.7, 110.2, 110.1, 69.3, 69.2, 69.1, 63.8, 31.8, 29.35, 29.3, 26.1, 22.7, 18.1, 14.1, 12.1 ppm; IR (neat): $\tilde{\nu}$ = 1692 cm^{-1} (C=O); elemental analysis calcd (%) for $C_{66}H_{104}O_7Si$ (1037.63): C 76.40, H 10.10; found: C 76.33, H 9.86.

Compound D2: As described for **D1**, with **3** (240 mg, 0.72 mmol), **9** (340 mg, 0.33 mmol), and *t*BuOK (89 mg, 0.80 mmol). The mixture was subjected to column chromatography on silica gel three times (CH_2Cl_2/hexane 1:4) to yield **D2** (150 mg, 33%) as an orange-red glassy product. ^{1}H NMR ($CDCl_3$, 300 MHz): δ = 7.67 (d, J = 8 Hz, 1H), 7.64 (s, 1H), 7.49 (d, J = 16.5 Hz, 2H), 7.42 (d, J = 8 Hz, 4H), 7.39 (m, 3H), 7.26 (d, J = 16.5 Hz, 2H), 7.16 (d, J = 16.5 Hz, 2H), 1.08 (s, 2H), 7.05 (d, J = 16.5 Hz, 2H), 6.68 (d, J = 8 Hz, 4H), 4.97 (s, 2H), 4.05 (m, 8H), 3.39 (q, J = 7 Hz, 8H), 1.86 (m, 8H), 1.31 (m, 40H), 1.19 (t, J = 7 Hz, 12H), 1.13 (m, 21H), 0.89 ppm (m, 12H); ^{13}C NMR ($CDCl_3$, 75 MHz): δ = 151.3, 150.7, 147.3, 138.5, 137.0, 135.2, 129.0, 128.3, 128.1, 127.9, 126.1, 125.9, 125.6, 125.5, 125.45, 125.4, 125.3, 124.9, 124.7, 123.2, 118.55, 118.5, 118.45, 111.7, 111.1, 111.05, 110.0, 69.8, 69.6, 63.8, 44.4, 31.8, 29.6, 29.55, 29.53, 29.45, 29.4, 29.35, 29.3, 26.35, 26.3, 26.2, 22.7, 22.65, 18.2, 14.1, 12.7, 12.1 ppm; elemental analysis calcd (%) for $C_{88}H_{134}N_2O_5Si$ (1328.13): C 79.58, H 10.17, N 2.11; found: C 79.26, H 10.57, N 1.90.

Compound 10: As described for **5**, with **D2** (100 mg, 0.08 mmol) and TBAF (0.10 mmol). Column chromatography on silica gel (CH_2Cl_2/hexane 2:1) yielded **10** (65 mg, 70%) as an orange-red glassy product. ^{1}H NMR ($CDCl_3$, 300 MHz): δ = 7.67 (d, J = 8 Hz, 1H), 7.64 (s, 1H), 7.49 (d, J = 16.5 Hz, 2H), 7.42 (d, J = 8 Hz, 4H), 7.39 (m, 3H), 7.26 (d, J = 16.5 Hz, 2H), 7.16 (d, J = 16.5 Hz, 2H), 7.08 (s, 2H), 7.05 (d, J = 16.5 Hz, 2H), 6.68 (d, J = 8 Hz, 4H), 4.88 (d, J = 5 Hz, 2H), 4.05 (m, 8H), 3.39 (q, J = 7 Hz, 8H), 1.86 (m, 8H), 1.31 (m, 40H), 1.19 (t, J = 7 Hz, 12H), 0.89 ppm (m, 12H); ^{13}C NMR ($CDCl_3$, 75 MHz): δ = 151.5, 151.3, 150.7, 147,3, 137.9, 137.3, 135.8, 129.15, 129.1, 128.5, 128.3, 127.9, 127.7, 126.8,

126.1, 126.0, 125.9, 125.7, 125.5, 125.4, 124.4, 123.6, 118.5, 111.7, 111.5, 110.9, 110.1, 109.8, 69.9, 69.8, 69.6, 69.5, 63.8, 44.4, 31.8, 29.7, 29.6, 29.6, 29.5, 29.4, 29.3, 22.7, 14.15, 12.7 ppm; elemental analysis calcd (%) for $C_{79}H_{114}N_2O_5$ (1171.78): C 80.98, H 9.81, N 2.39; found: C 80.47, H 9.87, N 2.04.

Compound F-D2: As described for **F-D1**, with **6** (74 mg, 0.06 mmol), **10** (60 mg, 0.05 mmol), DCC (25 mg, 0.12 mmol), and DMAP (1.2 mg, 0.01 mmol). Column chromatography on silica gel (CH_2Cl_2/hexane 1:3) yielded **F-D2** (75 mg, 60%) as a dark brown glassy product. ^{1}H NMR ($CDCl_3$, 300 MHz): $\delta = 7.67$ (d, $J = 8$ Hz, 1H), 7.54–7.34 (m, 10H), 7.28 (d, $J = 16.5$ Hz, 2H), 7.16 (d, $J = 16.5$ Hz, 2H), 7.09 (s, 2H), 7.05 (d, $J = 16.5$ Hz, 2H), 6.68 (br d, $J = 7$ Hz, 4H), 6.54 (d, $J = 2$ Hz, 2H), 6.36 (t, $J = 2$ Hz, 1H), 5.46 (s, 2H), 5.34 (s, 2H), 5.00 (s, 2H), 4.02 (m, 8H), 3.84 (t, $J = 7$ Hz, 4H), 3.39 (q, $J = 7$ Hz, 8H), 1.86 (m, 8H), 1.70 (m, 4H), 1.30 (m, 76H), 1.19 (t, $J = 7$ Hz, 12H), 0.89 ppm (m, 18H); ^{13}C NMR ($CDCl_3$, 75 MHz): $\delta = 166.5$, 163.0, 162.9, 160.4, 151.4, 151.3, 150.7, 147.3, 145.15, 145.1, 145.0, 144.95, 144.9, 144.8, 144.6, 144.5, 144.4, 144.2, 143.8, 143.75, 143.0, 142.95, 142.9, 142.85, 142.8, 142.7, 142.2, 142.1, 141.8, 141.7, 140.8, 140.7, 139.8, 138.3, 137.4, 136.6, 131.9, 129.2, 129.1, 128.8, 128.6, 128.4, 127.95, 127.9, 127.3, 126.6, 126.4, 126.3, 126.25, 126.2, 125.6, 125.45, 125.4, 124.1, 123.6, 118.5, 111.7, 111.1, 110.95, 110.9, 110.0, 109.9, 107.2, 101.7, 71.1, 69.7, 69.5, 69.4, 69.0, 68.1, 65.8, 62.7, 62.5, 44.4, 31.9, 31.8, 29.7, 29.6, 29.55, 29.5, 29.45, 29.4, 29.35, 29.3, 29.25, 26.5, 26.4, 26.3, 26.2, 22.75, 22.7, 14.1, 12.7 ppm; IR (neat): $\tilde{\nu} = 1747$ cm^{-1} (C=O); MALDI-TOF MS: m/z: calcd for $C_{175}H_{170}N_2O_{12}$: 2493.28; found 2493.0 $[M]^+$; elemental analysis calcd (%) for $C_{175}H_{170}N_2O_{12}$ (2493.28): C 84.30, H 6.87, N 1.12; found: C 84.43, H 6.71, N 1.05.

Electrochemistry: The cyclic voltammetric measurements were carried out using a potentiostat Autolab PGSTAT100. Experiments were performed at room temperature in a homemade airtight three-electrode cell connected to a vacuum/argon line. The reference electrode consisted of a saturated calomel electrode (SCE) separated from the solution by a bridge compartment. The counter electrode was a platinum wire of approximately 1 cm^2 apparent surface. The working electrode was a Pt microdisc (0.5 mm diameter). The supporting electrolyte [nBu$_4$N][BF$_4$] (Fluka, 99% electrochemical grade) was used as received and simply degassed under argon. Dichloromethane was freshly distilled over CaH_2 prior to use. The solutions used during the electrochemical studies were typically 10^{-3} M for the compound and 0.1 M for the supporting electrolyte. Before each measurement, the solutions were degassed by bubbling argon, and the working electrode was polished using a polishing machine (Presi P230). Under these experimental conditions, Fc^+/Fc was observed at ($+0.54 \pm 0.01$) V versus SCE.

X-ray crystal structure of D1: Crystals suitable for X-ray crystal-structure analysis were obtained by slow diffusion of EtOH into a solution of **D1** in $CHCl_3$. Data were collected at 180 K using a Xcalibur Oxford Diffraction diffractometer with graphite-monochromated $Mo_{K\alpha}$ radiation ($\lambda = 0.71073$ Å) and equipped with an Oxford Cryosystems Cryostream Cooler device. The structures were solved by direct methods using SIR92[28] and refined by means of least-squares procedures on F using the programs of the PC version of CRYSTALS.[29] Atomic scattering factors were taken from the International Tables for X-ray Crystallography.[30] The non-hydrogen atoms were anisotropically refined. Hydrogen atoms were located in a difference map, but those attached to carbon atoms were repositioned geometrically. All hydrogen atoms were refined using a riding model. $C_{40}H_{58}N_2OSi$ ($M_r = 611.00$); yellow block crystal; crystal size $0.10 \times 0.20 \times 0.40$ mm; triclinic; space group $P\bar{1}$; $a = 9.913(1)$, $b = 12.583(1)$, $c = 15.767(2)$ Å; $\alpha = 76.006(9)$, $\beta = 76.869(9)$, $\gamma = 76.070(8)°$; $V = 1822.2(3)$ Å^3; $Z = 2$; $\mu(Mo_{K\alpha}) = 0.096$ mm^{-1}; 17130 reflections measured; 9643 unique reflections ($R_{int} = 0.04$) and a total of 397 parameters were used. The final agreement factors were $R = 0.070$, $wR = 0.074$ for the 3993 reflections having $I > 3\sigma$. CCDC-728646 contains the supplementary crystallographic data for this paper. These data can be obtained free of charge from The Cambridge Crystallographic Data Centre via www.ccdc.cam.ac.uk/data_request/cif.

Photophysical measurements: The photophysical investigations were carried out in benzonitrile and toluene (Carlo Erba, spectrofluorimetric grade). Absorption spectra were recorded using a Perkin–Elmer λ40 spectrophotometer. Emission spectra were obtained using an Edinburgh FLS920 spectrometer (continuous 450 W Xenon lamp), equipped with a Peltier-cooled Hamamatsu R928 photomultiplier tube (185–850 nm) or a Hamamatsu R5509-72 supercooled photomultiplier tube (193 K, 800–1700 nm range). Emission quantum yields were determined according to the approach described by Demas and Crosby[31] using quinine sulfate in 1 N H_2SO_4 ($\Phi = 0.546$)[32] as standard. Emission lifetimes were determined with the time-correlated single-photon counting technique using an Edinburgh FLS920 spectrometer equipped with a laser diode head as excitation source (1 MHz repetition rate, $\lambda_{exc} = 407$ or 635 nm, 200 ps time resolution upon deconvolution) and an Hamamatsu R928 PMT as detector. Transient absorption spectra in the nanosecond/microsecond time domain were obtained by using the nanosecond flash photolysis apparatus described previously.[33] Experimental uncertainties are estimated to be 8% for lifetime determinations, 20% for emission quantum yields, 10% for relative emission intensities in the near-IR, and 1 and 5 nm for absorption and emission peaks, respectively.

Femtosecond time-resolved experiments were performed using a pump-probe setup based on the Spectra-Physics Hurricane Ti:sapphire laser source and the Ultrafast Systems Helios spectrometer.[34] The 550 nm pump pulses were generated with a Spectra Physics 800 OPA. Probe pulses were obtained by continuum generation on a sapphire plate. The effective time resolution was approximately 300 fs, the temporal chirp over the white-light 450–750 nm range was approximately 200 fs, and the temporal window of the optical delay stage was 0–1000 ps. The time-resolved spectral data were analyzed using the Ultrafast Systems Surface Explorer Pro software.[35]

Acknowledgements

This research was supported by the Centre National de la Recherche Scientifique (UMR 7509), the Agence Nationale de la Recherche (Solaire Photovoltaïque—Nanorgysol), the CNR (Commessa PM.P04.010, MACOL) and the EC through the Marie-Curie RTN PRAIRIES (MRTN-CT-2006-035810) and ITN FINELUMEN (PITN-GA-2008-215399). A.G. thanks the Agence de l'Environnement et de la Maîtrise de l'Energie—Région Alsace for her fellowship.

[1] D. M. Guldi, *Chem. Soc. Rev.* **2002**, *31*, 22–36; H. Imahori, *J. Phys. Chem. B* **2004**, *108*, 6130–6143; J.-F. Nierengarten, *Sol. Energy Mater. Sol. Cells* **2004**, *83*, 187–199; J.-F. Nierengarten, *New J. Chem.* **2004**, *28*, 1177–1191.

[2] J. L. Segura, N. Martin and D. M. Guldi, *Chem. Soc. Rev.* **2005**, *34*, 31–47; T. M. Figueira-Duarte, A. Gégout, J.-F. Nierengarten, *Chem. Commun.* **2007**, 109–119.

[3] T. M. Figueira-Duarte, J. Clifford, V. Amendola, A. Gégout, J. Olivier, F. Cardinali, M. Meneghetti, N. Armaroli, J.-F. Nierengarten, *Chem. Commun.* **2006**, 2054–2056.

[4] a) A. G. Avent, P. R. Birkett, F. Paolucci, S. Roffia, R. Taylor, N. K. Wachter, *J. Chem. Soc. Faraday Trans. 2* **2000**, 1409–1414; b) J. L. Segura, R. Gomez, N. Martin, C. P. Luo, A. Swartz, D. M. Guldi, *Chem. Commun.* **2001**, 707–708; c) M. Schwell, N. K. Wachter, J. H. Rice, J. P. Galaup, S. Leach, R. Taylor, R. V. Bensasson, *Chem. Phys. Lett.* **2001**, *339*, 29–35; d) F. Langa, M. J. Gomez-Escalonilla, E. Diez-Barra, J. C. Garcia-Martinez, A. de La Hoz, J. Rodriguez-Lopez, A. Gonzalez-Cortes, V. Lopez-Arza, *Tetrahedron Lett.* **2001**, *42*, 3435–3438; e) G. Accorsi, N. Armaroli, J.-F. Eckert, J.-F. Nierengarten, *Tetrahedron Lett.* **2002**, *43*, 65–68; f) D. M. Guldi, A. Swartz, C. P. Luo, R. Gomez, J. L. Segura, N. Martin, *J. Am. Chem. Soc.* **2002**, *124*, 10875–10886; g) J.-F. Nierengarten, N. Armaroli, G. Accorsi, Y. Rio, J.-F. Eckert, *Chem. Eur. J.* **2003**, *9*, 36–41; h) N. Armaroli, G. Accorsi, J. N. Clifford, J.-F. Eckert, J.-F. Nierengarten, *Chem. Asian J.* **2006**, *1*, 564–574; i) J. N. Clifford, A. Gégout, S. Zhang, R. Pereira de Freitas, M. Urbani, M. Holler, P. Ceroni, J.-F. Nierengarten, N. Armaroli, *Eur. J. Org. Chem.* **2007**, 5899–5908.

[5] M. Gutierrez-Nava, G. Accorsi, P. Masson, N. Armaroli, J.-F. Nierengarten, *Chem. Eur. J.* **2004**, *10*, 5076–5086.
[6] J.-F. Eckert, J.-F. Nicoud, J.-F. Nierengarten, S.-G. Liu, L. Echegoyen, F. Barigelletti, N. Armaroli, L. Ouali, V. Krasnikov, G. Hadziioannou, *J. Am. Chem. Soc.* **2000**, *122*, 7467–7479; N. Armaroli, F. Barigelletti, P. Ceroni, J.-F. Eckert, J.-F. Nicoud, J.-F. Nierengarten, *Chem. Commun.* **2000**, 599–600; F. Langa, M. J. Gomez-Escalonilla, J.-M. Rueff, T. M. Figueira Duarte, J.-F. Nierengarten, V. Palermo, P. Samorì, Y. Rio, G. Accorsi, N. Armaroli, *Chem. Eur. J.* **2005**, *11*, 4405–4415.
[7] a) E. Peeters, P. A. van Hal, J. Knol, C. J. Brabec, N. S. Sariciftci, J. C. Hummelen, R. A. J. Janssen, *J. Phys. Chem. B* **2000**, *104*, 10174–10190; b) D. M. Guldi, C. Luo, A. Swartz, R. Gomez, J. L. Segura, N. Martin, C. Brabec, N. S. Sariciftci, *J. Org. Chem.* **2002**, *67*, 1141–1152; c) D. M. Guldi, C. Luo, A. Swartz, R. Gomez, J. L. Segura, N. Martin, *J. Phys. Chem. A* **2004**, *108*, 455–467; d) A. M. Ramos, S. C. J. Meskers, P. A. van Hal, J. Knol, J. C. Hummelen, R. A. J. Janssen, *J. Phys. Chem. A* **2003**, *107*, 9269–9283.
[8] J. L. Segura, R. Gomez, N. Martin, C. Luo, D. M. Guldi, *Chem. Commun.* **2000**, 701–702.
[9] K. Müllen, G. Wegner, *Electronic Materials: the Oligomer Approach*, Wiley-VCH, Weinheim, **1998**.
[10] S. Zheng, S. Barlow, T. C. Parker, S. R. Marder, *Tetrahedron Lett.* **2003**, *44*, 7989–7992.
[11] A. Gégout, M. Holler, T. M. Figueira-Duarte, J.-F. Nierengarten, *Eur. J. Org. Chem.* **2008**, 3627–3634.
[12] U. Hahn, K. Hosomizu, H. Imahori, J.-F. Nierengarten, *Eur. J. Org. Chem.* **2006**, 85–91.
[13] F. Cardullo, P. Seiler, L. Isaacs, J.-F. Nierengarten, R. F. Haldimann, F. Diederich, T. Mordasini-Denti, W. Thiel, C. Boudon, J.-P. Gisselbrecht, M. Gross, *Helv. Chim. Acta* **1997**, *80*, 343–371; D. Felder, H. Nierengarten, J.-P. Gisselbrecht, C. Boudon, E. Leize, J.-F. Nicoud, M. Gross, A. Van Dorsselaer, J.-F. Nierengarten, *New J. Chem.* **2000**, *24*, 687–695; R. Pereira de Freitas, J. Iehl, B. Delavaux-Nicot, J.-F. Nierengarten, *Tetrahedron* **2008**, *64*, 11409–11419.
[14] U. Hahn, E. Maisonhaute, C. Amatore, J.-F. Nierengarten, *Angew. Chem.* **2007**, *119*, 969–972; *Angew. Chem. Int. Ed.* **2007**, *46*, 951–954.
[15] B. Knight, N. Martín, T. Ohno, E. Ortí, C. Rovira, J. Veciana, J. Vidal-Gancedo, P. Viruela, R. Viruela, F. Wudl, *J. Am. Chem. Soc.* **1997**, *119*, 9871–9882; R. Kessinger, J. Crassous, A. Herrmann, M. Rüttimann, L. Echegoyen, F. Diederich, *Angew. Chem.* **1998**, *110*, 2022–2025; *Angew. Chem. Int. Ed.* **1998**, *37*, 1919–1922; M. W. J. Beulen, L. Echegoyen, J. A. Rivera, M. A. Herranz, A. Martin-Domenech, N. Martin, *Chem. Commun.* **2000**, 917–918.
[16] T. Gu, P. Ceroni, G. Marconi, N. Armaroli, J.-F. Nierengarten, *J. Org. Chem.* **2001**, *66*, 6432–6439.
[17] T. Gu, D. Tsamouras, C. Melzer, V. Krasnikov, J.-P. Gisselbrecht, M. Gross, G. Hadziioannou, J.-F. Nierengarten, *ChemPhysChem* **2002**, *3*, 124–127.
[18] N. Armaroli, G. Accorsi, Y. Rio, J. F. Nierengarten, J. F. Eckert, M. J. Gomez-Escalonilla, F. Langa, *Synth. Met.* **2004**, *147*, 19–28.
[19] J.-F. Nierengarten, S. Zhang, A. Gégout, M. Urbani, N. Armaroli, G. Marconi, Y. Rio, *J. Org. Chem.* **2005**, *70*, 7550–7557.
[20] N. Clifford, T. Gu, J. F. Nierengarten, N. Armaroli, *Photochem. Photobiol. Sci.* **2006**, *5*, 1165–1172.
[21] D. M. Guldi, M. Prato, *Acc. Chem. Res.* **2000**, *33*, 695–703.
[22] H. Onodera, Y. Araki, M. Fujitsuka, S. Onodera, O. Ito, F. Bai, M. Zheng, J. L. Yang, *J. Phys. Chem. A* **2001**, *105*, 7341–7349.
[23] N. Armaroli in *Fullerenes: From Synthesis to Optoelectronic Properties* (Eds.: D. M. Guldi, N. Martin), Kluwer Academic, Dordrecht, **2002**, pp. 137–162.
[24] M. El-Khouly, M. Fujitsuka, O. Ito, M. El-Kemary, *J. Photochem. Photobiol. A* **2001**, *141*, 1–7.
[25] T. Nojiri, A. Watanabe, O. Ito, *J. Phys. Chem. A* **1998**, *102*, 5215–5219.
[26] T. Konishi, A. Ikeda, T. Kishida, B. S. Rasmussen, M. Fujitsuka, O. Ito, S. Shinkai, *J. Phys. Chem. A* **2002**, *106*, 10254–10260.
[27] M. J. Gomez-Escalonilla, F. Langa, J.-M. Rueff, L. Oswald, J.-F. Nierengarten, *Tetrahedron Lett.* **2002**, *43*, 7507–7511.
[28] A. Altomare, G. Cascarano, C. Giacovazzo, A. Guagliardi, *J. Appl. Crystallogr.* **1993**, *26*, 343–350.
[29] P. W. Betteridge, J. R. Carruthers, R. I. Cooper, K. Prout, D. J. Watkin, *J. Appl. Crystallogr.* **2003**, *36*, 1487.
[30] *International Tables for X-ray Crystallography, Vol. IV*, Kynoch Press, Birmingham, **1974**.
[31] J. N. Demas, G. A. Crosby, *J. Phys. Chem.* **1971**, *75*, 991–1024.
[32] S. R. Meech, D. Phillips, *J. Photochem.* **1983**, *23*, 193–217.
[33] L. Flamigni, *J. Phys. Chem.* **1992**, *96*, 3331–3337.
[34] C. Chiorboli, M. A. J. Rodgers, F. Scandola, *J. Am. Chem. Soc.* **2003**, *125*, 483–491.
[35] Surface Xplorer, analysis software for transient absorption data, Ultrafast Systems LLC, http://www.ultrafastsystems.com/surface_xplorer.htm

Received: May 7, 2009
Published online: July 27, 2009

